The modelling of multi-resonant thermally activated delayed fluorescence emitters – properly accounting for electron correlation is key!

David Hall,[a, b] Juan Carlos Sancho-Garcia,[c] Anton Pershin,[d] David Beljonne,[b] Eli Zysman-Colman[a] and Yoann Olivier[e*]*

[a]Organic Semiconductor Centre, EaStCHEM School of Chemistry, University of St Andrews, St Andrews, UK, KY16 9ST. E-mail: eli.zysman-colman@st-andrews.ac.uk; http://www.zysman-colman.com

[b]Laboratory for Chemistry of Novel Materials, University of Mons, 7000, Mons, Belgium.

[c]Department of Physical Chemistry, University of Alicante, E-03080, Alicante, Spain;

[d]Wigner Research Centre for Physics, PO Box 49, Budapest, Hungary;

[e]Laboratory for Computational Modeling of Functional Materials, Namur Institute of Structured Matter, Université de Namur, Rue de Bruxelles, 61, 5000 Namur, Belgium.

Abstract

With the surge of interest in multi-resonant thermally activated delayed fluorescent (MR-TADF) materials it is important that there exist computational methods to accurately model their excited states. Here, building on our previous work, we demonstrate how the Spin-Component Scaling second-order approximate Coupled-Cluster (SCS-CC2), a wavefunction-based method, is robust at predicting the ΔE_{ST} (i.e., the energy difference between the lowest singlet and triplet excited states) of a large number of MR-TADF materials, with a mean average deviation (MAD) of 0.04 eV compared to experimental data. Time-Dependent Density Functional Theory calculations with the most common DFT functionals as well as the consideration of the Tamm-Dancoff approximation (TDA) consistently predict a much larger ΔE_{ST} owing to the absence of an explicit account of double (or higher order) excitations. This

contribution is key in order to describe more precisely the Coulomb correlation that results in a stabilization of the S_1 state. We also employed SCS-CC2 to evaluate donor-acceptor systems that contain a MR-TADF moiety acting as the acceptor and show that the broad emission observed for some of these compounds arises from the solvent-promoted stabilization of a higher-lying charge transfer (CT) singlet state (S_2). This work highlights the importance of using wavefunction methods in relation MR-TADF emitter design and associated photophysics.

Introduction

Thermally activated delayed fluorescence (TADF) has received significant interest in recent years as materials showing TADF have been demonstrated to act as high-performance emitters in organic light-emitting diodes (OLEDs).[1-4] The mechanism is based on the thermal upconversion of triplet excitons into singlets via reverse intersystem crossing (RISC). Triplet harvesting in TADF provides a route to 100% internal quantum efficiency (IQE),[5] and a tantalizing alternative family of materials to the state-of-the-art phosphorescent emitters presently used in OLEDs. The design of TADF emitters focuses on the minimization of the energy gap (ΔE_{ST}) between the lowest singlet (S_1) and triplet (T_1) excited states.[6] Although for RISC to occur directly between these two states there must be spin-orbit coupling, and thus the two states must have different orbital type, satisfying El Sayed's rules,[7] ΔE_{ST} remains the primary metric that is optimized in TADF materials development. The most widely used strategy to ensure a small ΔE_{ST} is to couple electron rich (donor) and electron poor (acceptor) fragments together covalently (D-A systems) but in a manner where the molecule adopts a highly twisted conformation[5] as this will permit sufficient decoupling of the hole and electron densities associated with the T_1 and S_1 excitations.

The huge range of materials showing TADF has been driven in part by the predictive power of time dependent density functional theory (TD-DFT) to ably predict ΔE_{ST} at low computational cost. Employing the Tamm-Dancoff approximation (TDA-DFT) to TD-DFT provides for a more accurate description of the triplet state and thus also ΔE_{ST}, addressing the triplet instability issue present in TD-DFT.[8] Typically, these methods are based on calculations of vertical excitations at the ground state optimized geometry, which mimic absorption; however, this is often the preferred approach adopted to

describe also the excited state properties of TADF materials, as optimizing excited states is more time consuming.[9] Notably, the diversity of available exchange-correlation functionals often leads to a large range of values for ΔE_{ST}.[10] In the TADF field, several reports exist for D-A systems, showcasing the advantages of some DFT approaches over others.[8, 11] Benchmarking DFT functionals against a reference method (often a wavefunction-based method) is necessary in order to make sure a given exchange-correlation can be safely applied to a new class of materials. This way of benchmarking has the advantage of directly comparing similar energy magnitudes in absence of vibronic and/or solvent effect, which might differ from one experimental study to another, thus making a non-biased comparison difficult.

Within the TADF community calculations centre around the use of hybrid functionals such as B3LYP and PBE0, with an exact exchange (xc) contribution of 20%[12] and 25%,[13] respectively. Although reports indicate these methods over stabilise charge transfer (CT) states,[11] they remain popular as they produce good agreement between experimentally determined and calculated ΔE_{ST}. However, it must be noted that these agreements essentially arise due to a compensation of errors, and recent work by Champagne and co-workers has suggested that they perform poorly when describing intermediate excited states.[14] Other popular hybrid functionals used include M06-2X, (exact exchange contribution of 54%),[15] which has been shown to improve the correction for the over stabilisation of CT states.[14] Range-separated functionals have also been used. In these methods the exchange potential varies depending on whether electron-electron interaction is considered to be long range or short range, with the former dominated by exact-exchange and the latter mainly by DFT-like exchange. The range separation parameter ω defines the interelectronic distance (r_{12}) where electron-electron interaction switches from short- to long-range. The default value of ω is fixed to 0.400 $Bohr^{-1}$ and 0.330 $Bohr^{-1}$ for LC-ωPBE and CAM-B3LYP functionals, respectively. For LC-ωPBE, short range interactions are described purely using DFT and long-range electron-electron interactions are described only considering exact-exchange. In CAM-B3LYP, short- and long-range interactions are described by a combination of both DFT and exact-exchange methods. The value of ω is expected to be materials-dependent and is often tuned

following the protocol proposed by Sun *et al.*[11] The LC-ω*PBE functional is the ω-tuned version of LC-ωPBE.

Multiresonant TADF (MR-TADF) compounds, an alternative class of TADF materials to D-A compounds, were first introduced by Hatakeyama *et al.*[16, 17] These compounds are designed through site-specific doping of electron donating atoms (e.g., nitrogen and oxygen) or withdrawing atoms/functional groups (e.g., boron and ketone groups) of nanographene-like compounds, which leads to a reduction of the exchange interaction and so ΔE_{ST}.[17] In contrast to D-A TADF emitters, the oscillator strength of MR-TADF compounds remains large due to the relatively larger overlap of the HOMO and LUMO wavefunctions (Figure **1**. MR-TADF materials have a series of distinct properties because of their rigid structures. They show very narrow emission profiles and have small Stokes shifts as there is only minimal reorganisation between ground and excited states;[16] they also typically exhibit high photoluminescence quantum yields, Φ_{PL}, due to a synergy between reduced non-radiative decay and increased radiative decay rates, and they show only a minimal positive solvatochromism owing to the short-range CT (SRCT) nature of the excited states.[18]

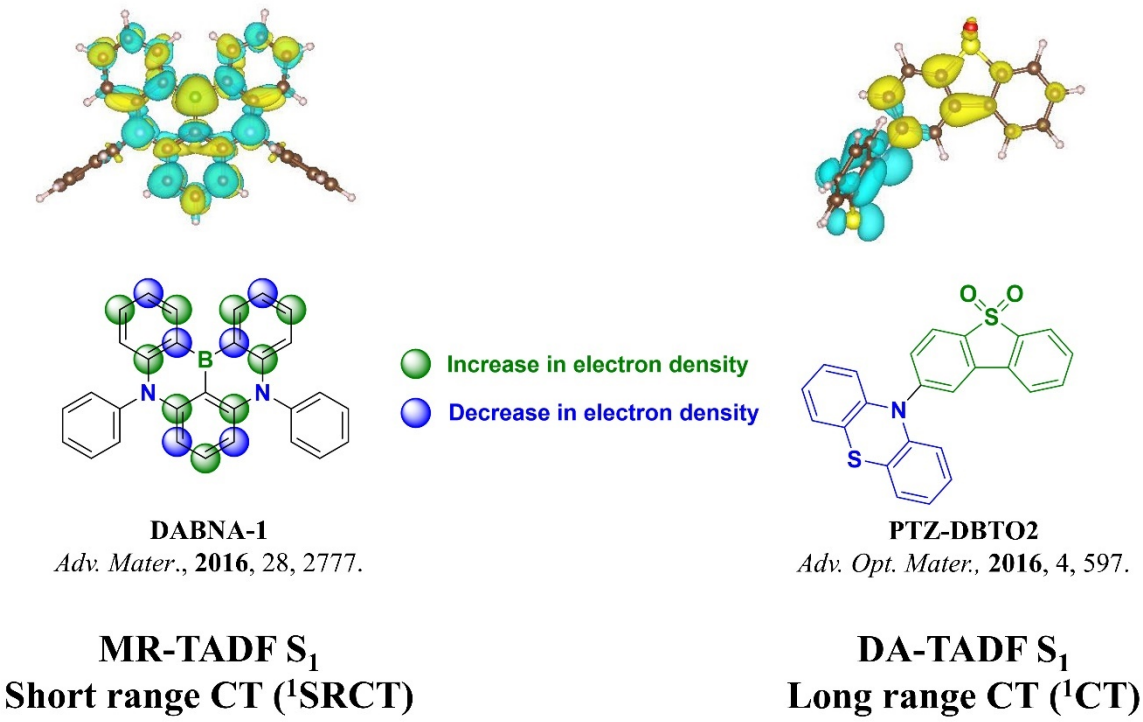

Figure **1**. Calculated and simplified difference density plots of the S_1 excited state of prototypical MR-TADF and D-A TADF compounds, (isovalue = 0.001).

We recently showed that the poor TD(A)-DFT prediction of ΔE_{ST} can be overcome by relying on wavefunction-based methods[19] [20, 21] and especially to the Spin-Component Scaling second-order approximate Coupled Cluster (SCS-CC2) approach.[22] Spin-component scaled (SCS) is a scaling factor introduced for distinguishing between the same spin and opposite spin interactions, resulting in an improved description of correlation effects.[23, 24] Coupled cluster calculations can include higher-order excitations (double, triple, etc.) either as a perturbation or through a non-perturbative approach starting from the Hatree-Fock reference wavefunction. The partial inclusion of double excitations within SCS-CC2, which are neglected in TD(A)-DFT, is the primary reason for the greater accuracy in predicting ΔE_{ST}, especially in these compounds, where the S_1 state is stabilized thanks to a better description of the Coulomb correlation interaction. However, the increase in accuracy, thanks to the inclusion of higher order electronic excitations, results in an increase in computational cost. The computational time of coupled-cluster calculations with single and double excitations (CCSD) scale with N^6, where N is a

number of basis functions, which is related to the system size. The computational time can be reduced somewhat to N^5 for CC2 as double excitations are partially included.[25] We initially demonstrated that SCS-CC2 calculations provided good agreement between experimental and computed ΔE_{ST} for two literature MR-TADF compounds, **DABNA-1** and **TABNA** (**2a**) (Figure 2).[19] We have since used the same methodology to accurately predict the ΔE_{ST} of several other MR-TADF emitters,[18, 26-28] and note that SCS-CC2/cc-pVDZ offers a good balance between accuracy and cost.[18, 26-28] In particular, we were able to compute the accurate values of ΔE_{ST} for the emitters, consisting of more than 100 atoms. Noteworthy, the scaling factor of coupled cluster methods can be reduced even further to N^4 with a spin-opposite scaling (SOS) method,[29] providing a correlated treatment for even larger systems at the costs comparable to TD-DFT. We also acknowledge that second-order algebraic diagrammatic construction (ADC(2))[30] and SCS-ADC(2)[20] that include partially double excitation have also been applied to MR-TADF with some success. However, since these methods account for the doubles in the same vein as SCS-CC2, they are not included in this study.

From a computational point of view, an organic emitter is often assigned to be MR-TADF on the basis of (i) the degree to which the HOMO and LUMO orbital distributions are complementary and (ii) the S_1 oscillator strength, often much larger than D-A systems.[17] However, these parameters do not permit assignment of the SRCT excited state with sufficient accuracy that is the hallmark of MR-TADF emitters, an assignment that is commonly accessible through analysis of the difference density plots. The frequent absence of predicted ΔE_{ST} in the MR-TADF literature is likely an implicit recognition that TD-DFT calculations do not accurately predict this value. From an experimental point of view, in addition to the observed thermally-activated delayed fluorescence, MR-TADF behaviour is frequently based on (i) the characterization of the full width at half maximum (FWHM) of the emission spectrum, which is expected to be narrow and (ii) on a small degree of positive solvatochromism. However, these are diagnostic, respectively, only of the rigidity of the compound (*i.e.,* small reorganization of the geometry in the excited state) and of a weakly CT electronic transition. Thus, these criteria should not be used exclusively to infer that the compound is indeed a MR-TADF emitter.

In this work, we have therefore computed the ΔE_{ST}, from the S_1 and T_1 energies of 35 reported MR-TADF emitters at the SCS-CC2/cc-pVDZ level, as well as with TD-DFT and TDA-DFT methods using a wide range of functionals, such as CAM-B3LYP, LC-ωPBE, LC-ω*PBE, B3LYP, PBE0 and M06-2X, all using the 6-31G(d,p) basis set, and the values directly compared to experiment. We quantify the accuracy of the predictions by assessing the mean average deviation (MAD). Our study reveals that TD-DFT in either its full treatment or within TDA completely fails to accurately predict ΔE_{ST}, and that the only way to reach a close agreement with the experiment is through the inclusion of double excitation or higher order excitation that is obtained here using the SCS-CC2 method. Indeed, there is a remarkable MAD of 0.04 eV for predicted ΔE_{ST} across the 35 emitters when SCS-CC2/cc-pVDZ is used, while DFT methods do very poorly, reflected in MAD values roughly ranging between 0.3 eV and 1.0 eV. The primary reason for the failure of DFT methods lies in the poorly predicted S_1 energies. We probed the manifolds of the singlet and triplet excited states of each material with the SCS-CC2 method. We observed that an increase in electronic delocalisation leads to a reduction in ΔE_{ST}. Interestingly, ketone-based MR-TADF emitters overall display the largest predicted ΔE_{ST} values. We also observed that very few emitters possess intermediate triplet states between S_1 and T_1. As reported by Kim et *al.*,[31] the RISC mechanism operating in MR-TADF compounds is likely more complex than only invoking T_1-T_2 vibronic coupling and might involve higher-lying triplet states, which results in a slower RISC in comparison to D-A TADF emitters. Often k_{RISC} of MR-TADF emitters is significantly higher in doped films than in solution where sometimes TADF is not observed. Recently, Wu *et al.*[32] suggested that depending on the electronic structure of the host material and the MR-TADF emitter, an exciplex between a MR-TADF emitter and the host could be formed. RISC is expected to take place from this exciplex and not directly on the emitter. We used the same methodology to investigate the nature of the excited states of 12 compounds that contain a MR-TADF unit acting as an acceptor in a D-A emitter design. In three of these compounds the CT nature of S_1 is captured. In the nine other compounds, we observed an inversion between the ^{1}CT (S_2) and ^{1}SRCT states in comparison to the experiment. Indeed, the S_2 state is calculated to be relatively close in energy to S_1, and thus given the solid-state polarization or solvent effects, it is not unexpected that the ^{1}CT state is the lowest singlet state observed experimentally.

Methodology

Each of the geometries of the 35 MR-TADF emitters was optimized using each of the aforementioned functionals in combination with the 6-31G(d,p) basis set for the DFT methods and the cc-pVDZ basis set for the SCS-CC2 calculations. Note that although cc-pVDZ is a basis set of moderate size, however, SCS-CC2 calculations used together with this basis are sufficiently close to those obtained with the larger and more costly def2-TZVP basis set.[22] The DFT functionals used consist of long range corrected (CAM-B3LYP[33] and LC-ωPBE[34]), optimally tuned LC-ωPBE (LC-ω*PBE[11]) and hybrid functionals (PBE0, [35] B3LYP[36] and M06-2X[15]). Excited state energies were calculated using TD-DFT and TDA-DFT.[8, 11, 37] For both SCS-CC2 and DFT methods, vertical excitations from the ground to the excited states were calculated. Such calculations are expected to reasonably accurately model the experimentally measured emission energies owing to the small observed Stokes shifts and limited positive solvatochromism. DFT calculations were performed using Gaussian 16[38] while SCS-CC2 was performed using Turbomole 7.4.[39]

For each method we report the MAD, root mean square deviation (RMSD) and standard deviation (σ) for S_1, T_1 and ΔE_{ST} over the set of 35 compounds. These are determined according to equations 3-5, respectively:

$$\text{MAD} = \frac{1}{n}\sum_{i=1}^{n}|x_i| \qquad (3)$$

$$\text{RMSD} = \sqrt{\frac{1}{n}\sum_{i=1}^{n}|x_i|^2} \qquad (4)$$

$$\sigma = \sqrt{\left(\frac{1}{n}\sum_{i=1}^{n}|x_i|^2\right) - \left(\frac{1}{n}\sum_{i=1}^{n}|x_i|\right)^2} \qquad (5)$$

Where $x_i = y_i^{Experiment} - y_i^{Calculated}$, with $y_i^{Experiment}$ being S_1, T_1, ΔE_{ST} obtained from the peak maxima (or the difference thereof) of the fluorescence and phosphorescence spectra in toluene glass at low temperature (frequently at 77 K). Where possible, we have compared to experimental data obtained under the same experimental conditions to maintain consistency in our analysis. $y_i^{Calculated}$ refers to the corresponding SCS-CC2, TD(A)-DFT calculations for S_1, T_1 or ΔE_{ST}, and i is the index over the

series of n = 35 studied molecules. Linear regression analysis was used to assess the predictive power of each method compared to experimental data. A secondary MAD was used to permit cross-comparison between the DFT-calculated oscillator strength and that calculated using SCS-CC2, wherein $x_i = y_i^{SCS-CC2} - y_i^{DFT}$.

Difference density plots, Δ, were obtained at the SCS-CC2 level. We define Δ_{sing} as the value of Δ obtained from SCS-CC2 calculations when only the single excitation contribution is considered, which provides a better comparison with TD(A)-DFT and a clearer picture for D-A systems. The attachment and detachment densities were calculated for each DFT functional at both TD-DFT and TDA-DFT levels of theory; these are associated with hole and electron densities. The densities are obtained through a post-analysis of the Gaussian outputs with the NANCY-EX 2.0 software.[40, 41] They can be related to the difference density using the following equation:[42]

$$\Delta = \mathrm{A} - \mathrm{D} \qquad (6)$$

where A is the attachment density and D is the detachment density. Comparisons between the nature of S_1 states between SCS-CC2 and DFT were made when comparing Δ with Δ_{sing}. A summary of the emitter structures is in Figure **2** and their photophysical properties are summarized in Table **S1**.

A design strategy that has been invoked to try and avoid aggregation-caused quenching (ACQ)[18] and/or to enable colour tuning[43-46] is to decorate the core MR-TADF structure with either bulky or electron-donor groups, respectively. These groups may affect the nature of the lowest-lying excited states by preferentially stabilizing a CT state over the SRCT state that is localized on the MR-TADF core, resulting in a broadening of the emission and the emergence of a strong positive solvatochromism. To probe this effect, we modelled 12 emitters that contain a MR-TADF core, which may act as an acceptor, and are decorated with pendant electron-donor groups. In each instance the ground state was optimized at the SCS-CC2/cc-pVDZ level of theory, vertical excitation calculations, including S_1, S_2, T_1 and T_2 were performed for each material. The D_{CT}, q_{CT} and S_{+-} descriptors were calculated for each emitter in order to distinguish between CT and SRCT states. The first metric, D_{CT}, is the distance between barycentres of the ρ_- (R_-) and ρ_+ (R_+). The larger is D_{CT} the greater is the CT character of the transition,

with a CT state often quoted as having D_{CT} > 1.6 Å while an LE state is defined as having a D_{CT} < 1.6 Å.[47] This metric has some drawbacks for symmetric systems since for strong CT states, the barycentre positions are predicted to be close, leading to small D_{CT} and an unrealistic LE assignment of the nature of the excited state.[47 48] The second metric considered is the charge transferred (q_{CT}), which corresponds to the integrated change in electronic density (either ρ_+ or ρ_-) over the volume on which ρ_+ or ρ_- expand. A value of 1 indicates a CT state and 0 indicates a LE state. The final metric employed is the overlap S_{+-}, which considers the overlap between areas of increased electronic density ρ_+ and decreased electronic density, ρ_-. An overlap S_{+-} of 1 indicates a LE state, while a value of 0 corresponds to no overlap and thus a CT state. The literature photophysical properties of the emitters are collated in Table **S2**.

Results and discussion

1) **Benchmarking of MR-TADF emitters**

a) **ΔE_{ST} modelling**

Figure **2** shows the chemical structures of the MR-TADF materials selected for this study. The structural diversity of these emitters covers examples across both the full spectral range (λ_{PL} ranging from 390 nm to 672 nm) but also examples of containing BN(O), N(O)B, and NC=O cores. Photophyscial and device data of each of the modelled emitters can be found in Table **S1.**

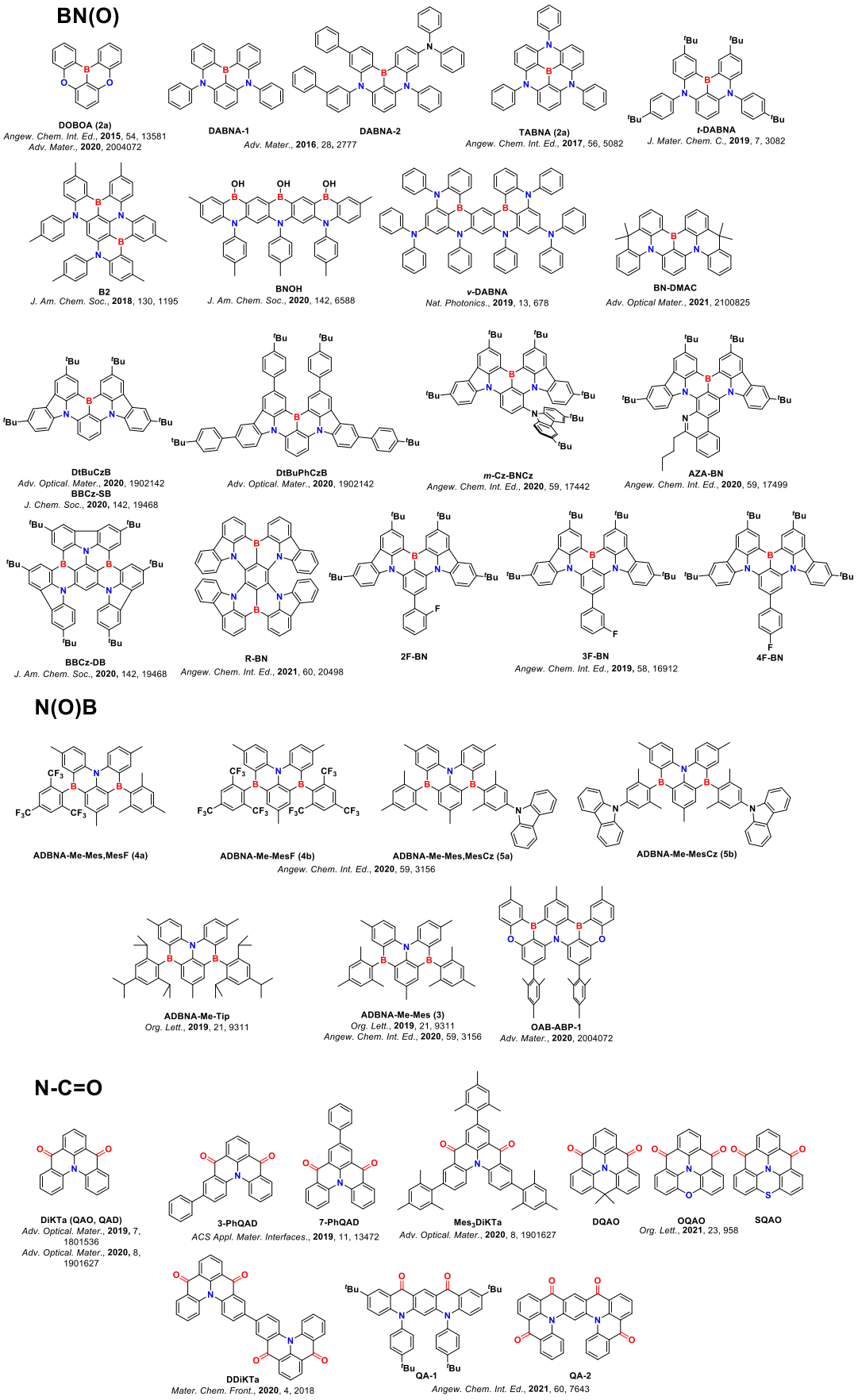

Figure **2**. Literature MR-TADF emitters modelled within this study.

TD-DFT or TDA-DFT calculations systematically and significantly overestimate ΔE_{ST}. There are, however, two exceptions, **ADBNA-Me-Mes-MesCz** (Table **S11** and Figure **S9a**) and **ADBNA-Me-MesCz** (Tables **S13** and **S11a**), where TDA-B3LYP/6-31 G(d,p) and TD-B3LYP/6-31 G(d,p) both perform well (the use of the PBE0 functional provides similar results). The experimentally determined ΔE_{ST} for **ADBNA-Me-Mes-MesCz** and **ADBNA-Me-MesCz** are 0.18 eV and 0.17 eV, respectively, in 1 wt% PMMA,[26] while TDA-B3LYP/6-31G(d,p) and TD-B3LYP/6-31G(d,p) estimated ΔE_{ST} to be, respectively, 0.28 eV and 0.26 eV for **ADBNA-Me-Mes-MesCz**, and 0.18 eV and 0.21 eV for **ADBNA-Me-MesCz**. ΔE_{ST} was predicted to be 0.17 eV for both compounds using SCS-CC2/cc-pVDZ, which are in excellent agreement with the experimental values. The excited state was assigned experimentally to be SRCT, which is well reproduced by SCS-CC2/cc-pVDZ (Figure **3a**) as Δ is localized on adjacent atoms. The SRCT nature was not captured by either TDA-B3LYP/6-31G(d,p) and TD-B3LYP/6-31G(d,p); instead, a ^{1}CT state was predicted (Figure **3b** and **S56**). The observation of an overstabilized CT state has been a well-documented weakness of DFT functionals such as B3LYP and PBE0, and is a consequence of a marked self-interaction error due to their low fraction of exact exchange.[11]

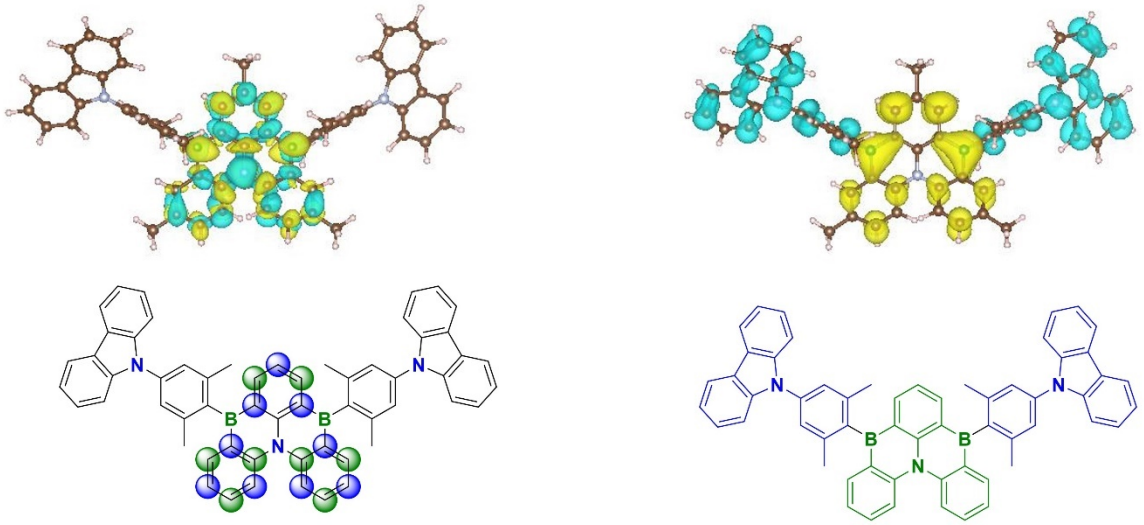

Figure **3**. Difference density plots calculated for **ADBNA-Me-MesCz** for the first singlet excited state with **a**) SCS-CC2/cc-pVDZ and **b**) TDA-B3LYP/6-31G(d,p), where blue balls represent decreased density and green balls increased density, (isovalue = 0.001).

Beyond these two emitters, the DFT calculated ΔE_{ST} was found to be consistently too high regardless of the functional employed; the long range corrected functionals CAM-B3LYP and LC-ωPBE were the poorest performing (see Table **1** for the MAD values). There is a slight but not significant improvement of the MAD when TDA-DFT calculations are used compared to the TD-DFT calculations, this due to an improved T_1 description.[8] When the ω value of LC-ωPBE is tuned for each emitter individually, a significant improvement in ΔE_{ST} becomes apparent, with the MAD dropping to 0.36 eV and 0.40 eV for TD-B3LYP/6-31G(d,p) and TDA-B3LYP/6-31G(d,p) calculations, respectively, values that are still much higher than those using SCS-CC2/cc-pVDZ (see Table **1**). A gradual decrease in the MAD is observed when hybrid functionals with decreasing exact exchange are employed, moving from 0.42 eV (0.44 eV), 0.35 eV (0.37 eV) to 0.29 eV (0.32 eV) for M06-2X, PBE0 and B3LYP using TD-DFT (TDA-DFT), respectively. This observation was previously reported by Pershin *et al.*, where the LDA

functional (with no exact-exchange) performing reasonably well for **DABNA-1** but at the expense of a wrongly predicted nature of the S_1 excited state.[22] When SCS-CC2 is applied, a remarkably small MAD of 0.04 eV is achieved for these compounds, along with a low σ of 0.001 eV. This vastly superior performance is testament to importance of the (partial) inclusion of double excitations, which is neglected in the TD(A)-DFT calculations.

Table **1**. Mean average deviation (MAD) and linear correlation coefficient (r^2) of T_1 and S_1 and ΔE_{ST} between computed and experimental data.

	CAM-B3LYP		LC-ωPBE		LC-ω*PBE		B3LYP		PBE0		M06-2X		SCS-CC2
	TD	TDA	TD	TDA	TD	TDA	TD	TDA	TD	TDA	TD	TDA	
MAD ΔE_{ST} / eV	0.55	0.51	0.98	0.62	0.36	0.40	0.29	0.32	0.35	0.37	0.42	0.44	0.04
r^2 ΔE_{ST} [a]	0.56	0.53	0.04	0.66	0.49	0.39	0.13	0.02	0.56	0.24	0.63	0.37	0.72
MAD S_1 / eV	0.90	0.99	1.22	1.33	0.47	0.54	0.35	0.41	0.46	0.52	0.86	0.94	0.55
r^2 S_1 [a]	0.89	0.94	0.95	0.96	0.88	0.87	0.80	0.73	0.92	0.92	0.90	0.93	0.98
MAD T_1 / eV	0.36	0.48	0.33	0.72	0.11	0.15	0.07	0.09	0.11	0.16	0.43	0.49	0.56
r^2 T_1 [a]	0.93	0.94	0.60	0.93	0.92	0.91	0.87	0.85	0.93	0.94	0.92	0.92	0.99

[a] Calculated considering only boron emitters

There is only a modest correlation (r^2 of 0.53 for SCS-CC2) between the experimentally determined and calculated ΔE_{ST} (Figure **S37a**). The r^2 increases to 0.72 when only the boron-containing emitters (Figure **4**) are included in the analysis. The poorer correlation found when the ketone-containing emitters are included can be understood as resulting from the greater degree of positive solvatochromism observed for these molecules compared to the boron-containing compounds (*vide infra*), which is not captured in our gas-phase calculations. Notably, our prediction for **BBCz-DB** (Figure ***4*b** blue circle) deviates considerably from the linear fit; it is not clear at this stage what is the origin of this deviation. Compared to SCS-CC2, TD(A)-DFT performs worse, with r^2 ranging between 0.02 and 0.66 when only the boron compounds are included in the data set (Figures **S38** – **43**, Table **S39**).

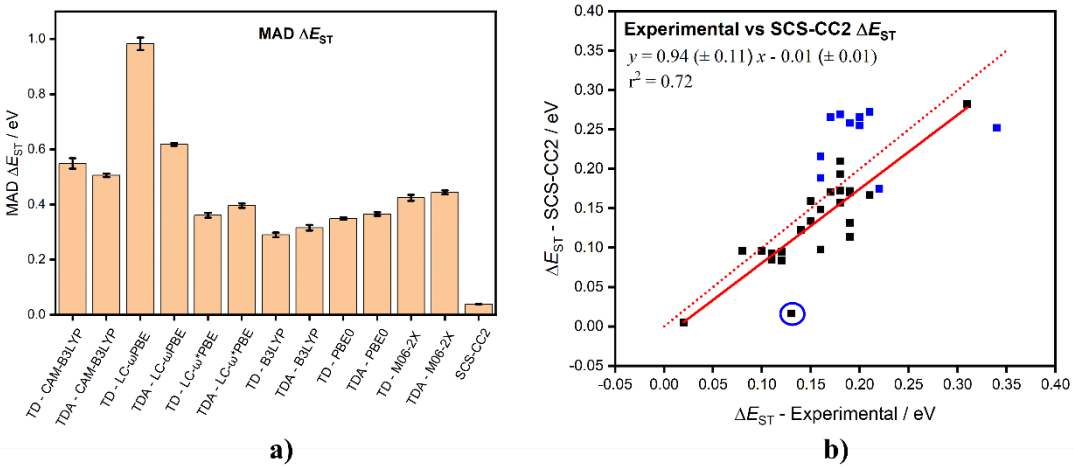

Figure **4**. **a)** ΔE_{ST} MAD comparing the different computational methodologies with experiment, and the associated error, **b)** Experimental vs SCS-CC2-calculated vertical ΔE_{ST}, where blue squares denote N-C=O emitters, the red solid line shows the trend line for the data with the N-C=O emitters excluded and the dotted red line represents the theoretical idealized fit. The blue circle corresponds to **BBCz-DB**, a boron-based emitter.

b) Excited state energies

In terms of materials development, it is not only important to accurately predict ΔE_{ST} but it is equally essential that the computational methodology accurately predicts the absolute energies of both the S_1 and T_1 states. Owing to the rigid character of MR-TADF compounds, there are small observed Stokes shifts,[16] which supports the use of vertical excitations based on a ground-state optimized geometry as a first approximation to calculating the lowest-lying excited state energies; the calculated values are thus higher in energy than those experimentally determined as medium effects are neglected in our calculations. Furthermore, the lack of significant observed positive solvatochromism in solution,[18] and the minimal impact of polarity in the solid state[49] implies that the inclusion of a solvent continuum model is not required for accurate predictions, thus gas phase calculations can be used as reasonable predictors for the optoelectronic properties of this class of emitter. For each of the DFT functionals, a large MAD for the S_1 energy was observed. This ranges between 0.90 eV and 1.33 eV when long range corrected functionals CAM-B3LYP and LC-ωPBE at both TD-DFT and TDA-DFT levels are

employed, decreasing to 0.47 eV and 0.54 eV, for TD-DFT and TDA-DFT respectively, when ω is tuned. When low exact exchange content hybrid functionals are employed, the MAD improves to 0.35 eV and 0.41 eV for B3LYP at TD-DFT and TDA-DFT respectively, rising to 0.46 eV and 0.52 eV for PBE0 at TD-DFT and TDA-DFT respectively. This increases to 0.86 eV and 0.94 eV at the TD-DFT and TDA-DFT levels for M06-2X. For SCS-CC2, the MAD for S_1 is 0.55 eV, which is similar to that for the low exact-exchange content functionals (Table **1**). There is a remarkable linear correlation (r^2 = 0.98) between experimental and SCS-CC2 calculated S_1 energies, when only including the boron-containing emitters are included in the data set (Figure **5a**). When the NC=O compounds are also included within the analysis, the r^2 is only 0.69 as in these emitters the influence from solvents and external polarisation are more pronounced. In addition, the influence of a difference in the geometrical relaxation between S_1 and T_1 excited states could be a reason for this deviation. For TD(A)-DFT, an improved correlation (r^2 ranging from 0.73 and 0.96) is apparent only when NC=O emitters are omitted; the r^2 ranges values are between 0.61 and 0.84 when all compounds are included in the study (Figures **S44**-**S49**, Tables **S40** and **S43**).

TD(A)-DFT calculations do a much better job of predicting the energy of the T_1 states, reflected in the much smaller MAD values (Figure **5d,** Table **1**). The smaller MAD observed at TD(A)-DFT for the T_1 in comparison to S_1 highlights the lesser importance of the contributions of double excitations in the description of the triplet state, due to a smaller contribution of the Coulomb correlation to the description of the triplet wavefunction. The SCS-CC2 T_1 MAD value is 0.56 eV, which is of the same order as the S_1 MAD (0.55 eV), this is the reason for the remarkably small ΔE_{ST} MAD (Figure **4b)** and thus predictive power of this methodology. Similarly, to the analysis employed for the comparison of the calculated and experimentally determined S_1 energies, there exists a strongly linear correlation for the T_1 energies (r^2 = 0.99) only when the NC=O emitters are excluded from the data set, with (Figure **5d**). Inclusion of the NC=O emitters results in a poorer correlation (r^2 = 0.71); the calculated T_1 states of the NC=O emitters are higher in energy than those experimentally determined (Figure **S37c**). DFT functionals perform well, with r^2 values surpassing 0.90 for 9 of the 12 functionals, again this analysis excludes the NC=O emitters (Table **S44**). Much like that observed for the S_1 analysis, the r^2 values (r^2

ranging from 0.50 – 0.86) decrease when the full data set is considered(Figures **S50** – **S55** and Tables **S41**).

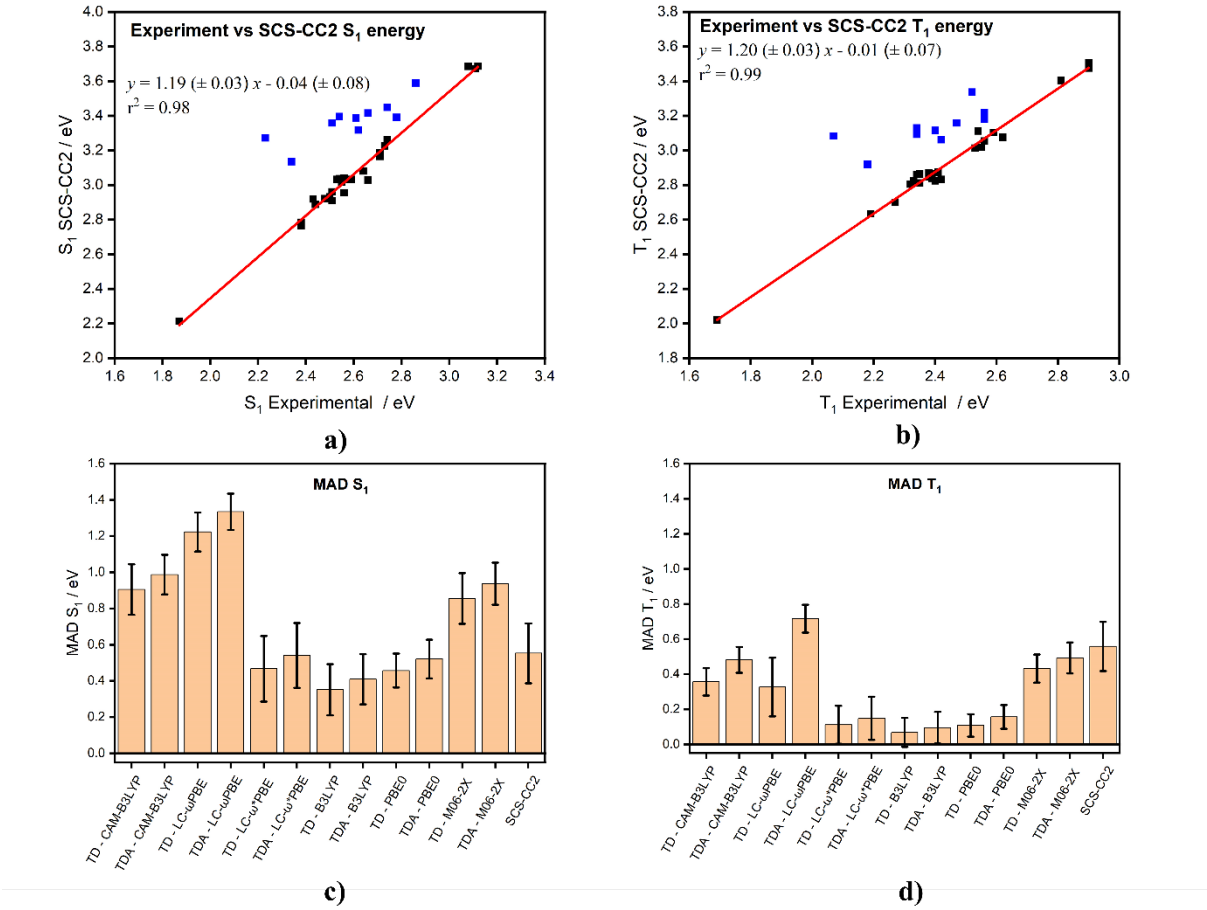

Figure **5**. **a)** S_1 and **b)** T_1 experimental vs SCS-CC2 vertical excitation energies for each emitter. The red lines correspond to a linear fit of the set of data when NC=O are omitted from the fitting and highlighted by blue squares. **c)** S_1 and **d)** T_1 MAD for both with respect to the experiment.

c) Oscillator strength and excited state nature

Taking the SCS-CC2 calculations as the reference method, we evaluated MAD as the difference between TD(A)-DFT calculated and the SCS-CC2 calculated oscillator strengths (Figure **6a**). The MAD values range from 0.04 with TD-CAM-B3LYP to 0.28 with TD-LC-ω*PBE. This analysis seems to suggest that TD(A)-DFT calculations predict a similar S_1 nature as the SCS-CC2 calculations as evidenced by the similar (yet not identical) difference density patterns in TD(A)-DFT and SCS-CC2

for most compounds. However, upon closer inspection we observe some significant discrepancies between the difference density patterns predicted between the DFT and SCS-CC2 calculations where for some systems, TD(A)-DFT calculations incorrectly assign S_1 has having either CT or n-π* character, when in fact the S_1 state shows SRCT character both experimentally and from the SCS-CC2 calculations. For instance, B3LYP and PBE0 both failed to predict the nature of the S_1 state of **ADBNA-Me-MesCz** and **ADBNA-Me-Mes-MesCz** (Figure **S56**). DFT methods such as TD(A)-DFT/LC-ωPBE, TDA-DFT/LC-ω*PBE or TD(A)-DFT do not accurately predict the SRCT nature of the S_1 state of a number of ketone-based MR-TADF compounds [**3-PhQAD** (Figure **S57**), **7-PhQAD** (Figure **S58**), **Mes$_3$DiKTa** (Figure **S59**), **DDiKTa** (Figure **S560**), **QA-2** (Figure **S61**), **DiKTa** (Figure **S62**) and **DQAO** (Figure **S63**)] and instead predict an S_1 state with n-π* character (Figure **7**); notably, SCS-CC2 predicts that the S_2 state for these compounds has n-π* character and so it appears that DFT methods overstabilize this state at the expense of the SRCT state. Due to the poor predictive ability of most DFT methods to accurately model the nature of the S_1 state, we would urge researchers to not routinely employ these methods for MR-TADF compounds as they may paint an erroneous picture of the excited state manifold. Of the DFT methods assessed, owing to its small MAD of 0.04 and small σ of 0.03, we would advocate the use of TD-CAM-B3LYP/6-31G(d,p) to capture S_1 excited state character if access to SCS-CC2 or other wavefunction-based methods are not available.

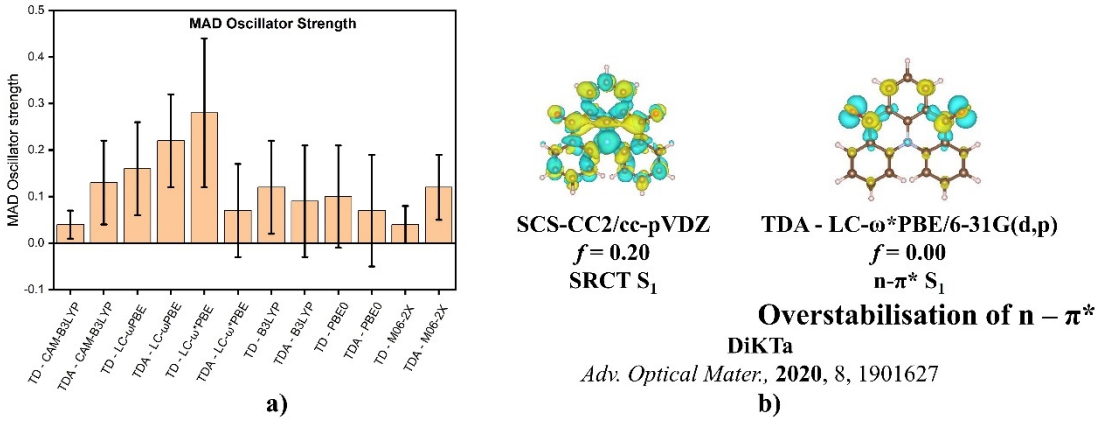

Figure **6**. Properties of S_1 nature between SCS-CC2 and DFT functionals, where **a)** is the MAD of the oscillator strength between SCS-CC2 and TD(A) – DFT and **b)** indicates the Δ of S_1 excited state of

DiKTa for SCS-CC2 and TDA-LC-ω*PBE showcasing the difference in the nature of this excited state and their calculated oscillator strength (*f*), (isovalue = 0.001).

d) Discussion on the RISC mechanism of MR-TADF emitters from an SCS-CC2 perspective

Our calculations with the SCS-CC2 method revealed that NC=O emitters have a larger predicted ΔE_{ST}, ranging between 0.17 eV and 0.27 eV while the boron-containing compounds (excluding **α-3BNOH**) have ΔE_{ST} ranging between 0.01 eV and 0.21 eV (Figure **8a**). When comparing **DiKTa** (ΔE_{ST} = 0.27 eV), **DABNA-1** (ΔE_{ST} = 0.16 eV) and **DOBNA** (ΔE_{ST} = 0.21 eV), **DiKTa** has the larger ΔE_{ST}. When analysing q_{CT} and D_{CT}, we observed that **DABNA-1** (**DiKTa**) S_1 and T_1 excited states exhibit the largest (lowest) CT character and thus the lowest (largest) ΔE_{ST} (see Table 2).

Table **2**. Charge transfer metrics for **DABNA-1**, **DOBNA** and **DiKTa** calculated with SCS-CC2/cc-pVDZ.

Compound	S_1		T_1		ΔE_{ST} / eV
	D_{CT} / Å	q_{CT}	D_{CT} / Å	q_{CT}	
DiKTa	0.81	0.59	0.61	0.59	0.27
DOBNA	0.84	0.57	0.68	0.61	0.20
DABNA-1	0.89	0.63	0.75	0.67	0.16

The largest ΔE_{ST} of the 35 compounds is observed for **α-3BNOH**, at 0.28 eV while the smallest calculated ΔE_{ST} are for ***ν*-DABNA** (0.01 eV) and **BBCz-DB** (0.02 eV). For the two former, this is likely due to the increased electronic delocalisation of the S_1 and T_1 excited states difference density (Figure *7*) minimizing the exchange interaction energy. We are uncertain as to the origin of the low ΔE_{ST} in **BBCz-DB** but note the unusually poor prediction compared to experimental ΔE_{ST} (Figure **4**, blue circle). **OAB-ABP-1** shows a smaller ΔE_{ST} of 0.08 eV compared to other nitrogen-centred emitters, likely linked to the extended π delocalisation afforded by the bridging oxygen atoms. This π-

delocalisation is the primary means to reduce ΔE_{ST}, and explains the modest decrease in ΔE_{ST} when carbazole moieties are incorporated into the molecule as in **2F-BN**, **3F-BN**, **4F-BN**, **DtBuCzBN**, **DtBuPhCzBN**, **m-CzBNCz** and **AZA-BN** compared to **DABNA-1**, (ΔE_{ST} 0.08 eV – 0.13 eV compared to 0.16 eV).

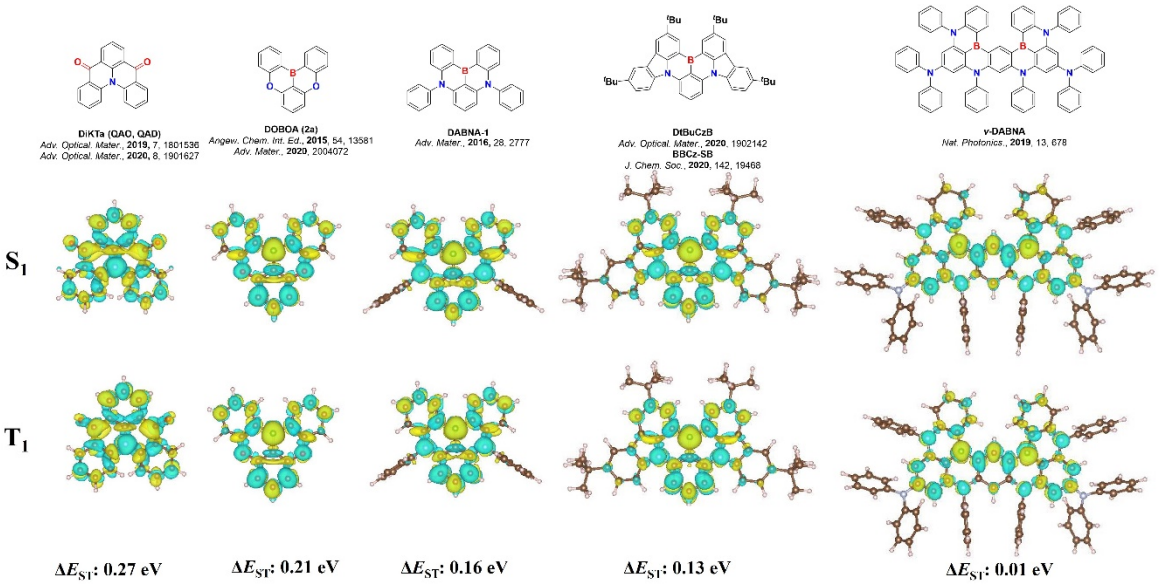

Figure **7**. Difference density patterns and ΔE_{ST} of calculated emitters, (isovalue = 0.001).

Similar character for the S_1 and T_1 states is observed for each of these emitters, based on an analysis of their difference density patterns (Figures **S64** – **S67**), which would suggest negligible SOC between these two states.[7] Thus in these compounds, a higher-lying triplet state must be involved in mediating RISC.[7, 50-52] In MR-TADF, RISC has been postulated to take place either via a super exchange mechanism,[31] or similarly as with D-A TADF materials via a spin-vibronic mechanism. For most of the compounds in this study the T_2 is calculated to be much higher in energy than S_1 (Figure **8c**), thus suggesting that its involvement in RISC is minimal. There are, however, five exceptions, namely **α-3BNOH**, **DDiKTa**, **B2**, **QA-1** and **QA-2**. Notably, **DDiKTa** and **QA-2** which all show very efficient RISC rates,[27, 28, 53] which is consistent with the involvement of T_2 facilitating RISC. Generally, smaller ΔE_{S1T2} is observed for the NC=O emitters (Figure **8**), which may explain the observed k_{RISC} values despite their larger calculated ΔE_{ST}. The position of higher-lying singlet states has also been conjectured to facilitate RISC in MR-TADF emitters;[54] however, in the majority of the examples S_2 is calculated to

be more than 0.4 eV destabilized compared to S_1 (Figure **8d**), rendering its influence to the RISC mechanism to be minimal. Several exceptions exist where each of **α-3BNOH**, **DDiKTa**, **B2**, **QA-1** and **QA-2** have low-lying S_2 states. We also note that ***ν*-DABNA** and **BBCz-DB** possess smaller calculated S_1-S_2 gaps. The similar nature of S_1 and T_1, and the large ΔE_{S1T2} and ΔE_{S2S1} may explain why MR-TADF emitters exhibit much slower k_{RISC} values than the highest performing D-A systems.

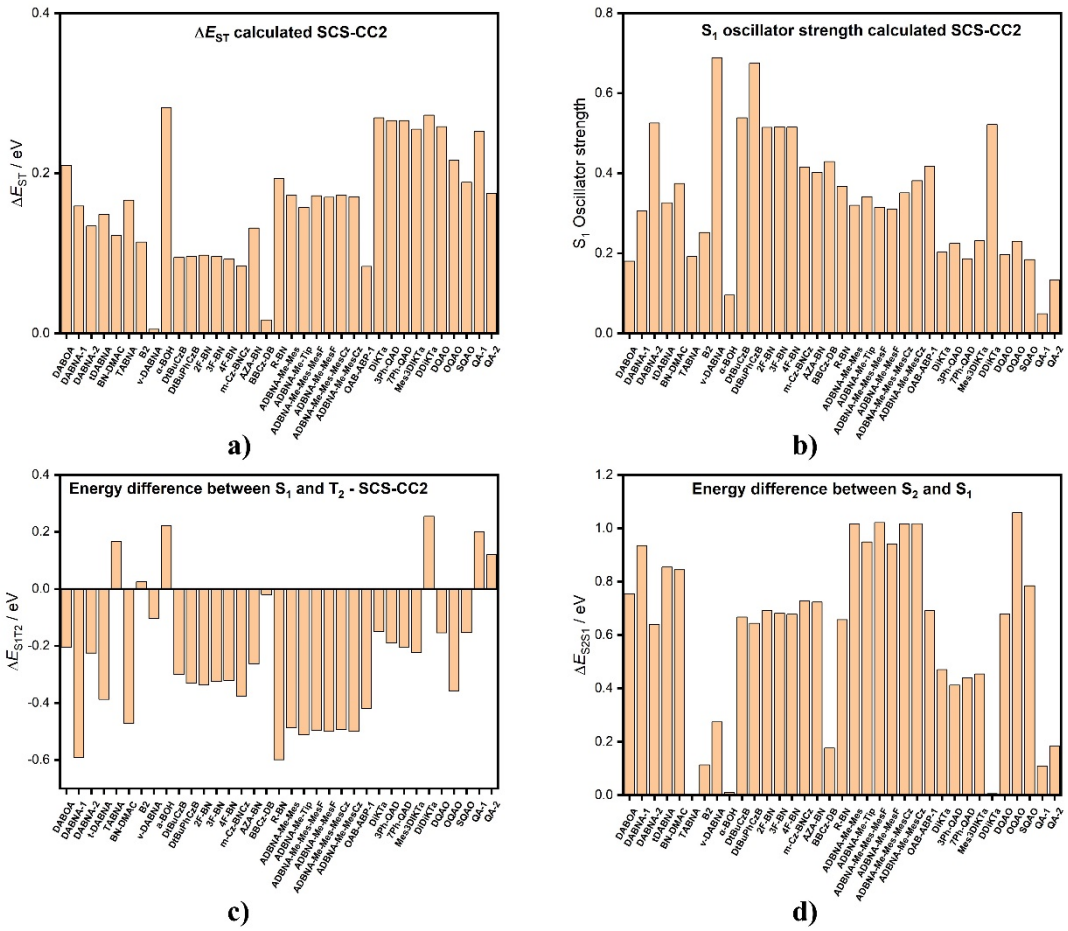

Figure **8**. Changing properties of each of the MR-TADF emitters calculated at SCS-CC2/cc-pVDZ, where **a)** is ΔE_{ST} , **b**) is S_1 oscillator strength, **c**) is the energy difference between S_1 and T_2 and **d)** is the energy difference between S_2 and S_1.

3) Modelling of emitters that contain MR-TADF core structures but that are not MR-TADF

An increasingly popular TADF molecular design is to use MR-TADF core structures as rigid acceptor units in formally D-A TADF systems.[26, 55-62] When a donor is sufficiently strong, the CT state becomes

the lowest lying state while the characteristic SRCT state of MR-TADF emitters is relegated to a higher lying excited state. The result of this design is a compound with an emission that is much broader and is more responsive to the polarity of the medium (Figure **1**) than conventional MR-TADF emitters.

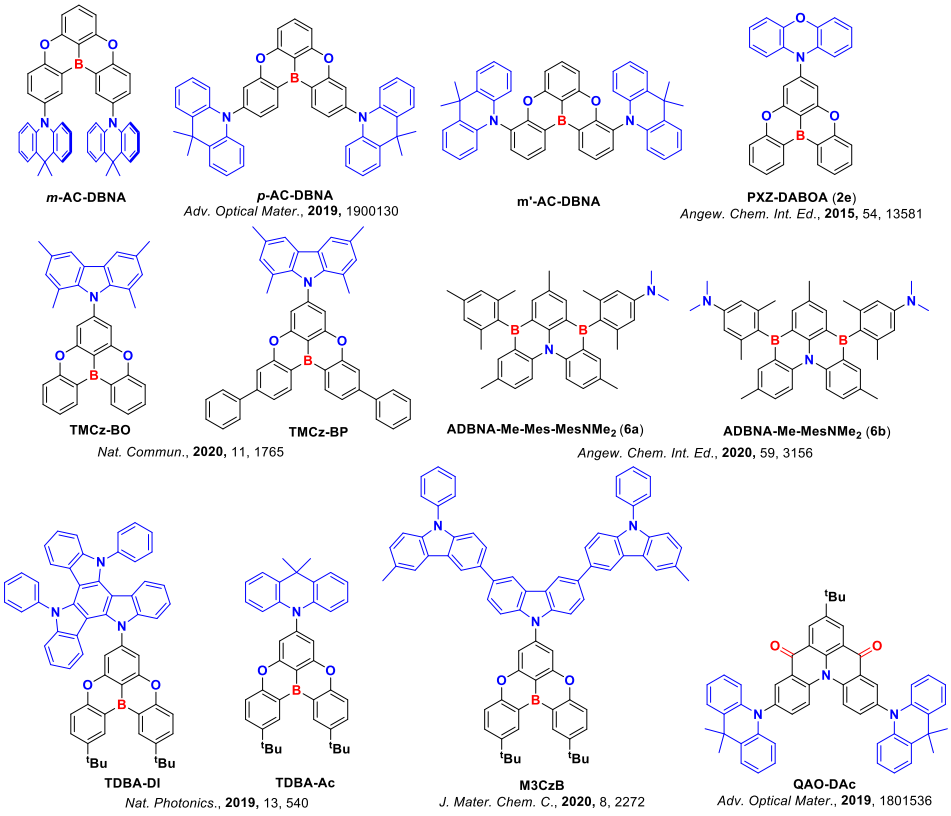

Figure **9**. Structures of modelled D-A TADF emitters which have a MR-TADF unit.

Recognizing the importance to accurately model the excited state manifold of this subclass of D-A systems, we performed SCS-CC2 calculations focussing on the nature of both the S_1 and S_2 states of 12 emitters, each of which containing a MR-TADF acceptor moiety but where experimentally the compound shows a broad emission spectrum and significant positive solvatochromism (Figure **9**). A full summary of the photophysical and device data can be found in Table **S2**. In each case, the degree of charge transfer character was determined, which acts as a metric for assigning the state as either SRCT or CT (Table **3** and **4**), along with the difference density plots (Figures **S68** – **S72**); the difference density plots of the MR-TADF moieties **DiKTa**, **DOBNA** and **ADBNA-Me-Mes** are shown in Figure **S68**. When employing a ground-state optimized geometry, SCS-CC2 incorrectly predicts a S_1 state with SCRT character for most of these compounds; only for **PXZ-DOBNA**, **m-AC-DBNA** and **p-AC-**

DBNA, do the SCS-CC2 calculations accurately predict the CT character of the S_1 state (Figure **S69,** Table **3**). Each of these three latter compounds contains the same common MR-TADF acceptor moiety based on **DOBNA**.

Table **3**. Calculated excited state natures of S_1 and S_2 for **DOBNA**, **PXZ-DOBNA**, **m-AC-DBNA** and **p-AC-DBNA**.

	S_1					S_2				
Compound	**Energy / eV**	**D_{CT} / Å**	**q_{CT}**	**S_{+-}**	**Excited state**	**Energy / eV**	**D_{CT} / Å**	**q_{CT}**	**S_{+-}**	**Excited state**
DOBNA	3.68	1.57	0.58	0.92	SRCT	N/A	N/A	N/A	N/A	N/A
PXZ-DOBNA	3.38	5.30	0.95	0.23	CT	3.67	1.31	0.58	0.94	SRCT
p-AC-DBNA	3.51	1.96	0.94	0.51	CT	3.52	1.95	0.94	0.51	CT
m-AC-DBNA	3.47	3.68	0.79	0.62	CT	3.52	4.34	0.91	0.32	CT

For nine of the emitters (**m'AC-DBNA**, **QAO-Dad**, **TBNA-Ac**, **TBNA-Di**, **ADBNA-Me-MesNMe2**, **ADBNA-Me-Mes-MesNMe2**, **TMCz-BO**, **TMCz-3P** and **M3CzB**) SCS-CC2 calculations predict a SRCT S_1 state, while a close-lying S_2 state displays pronounced CT character (Table and Figures **S70** – **S72**); the SRCT nature of the S_1 state is based on the similar D_{CT}, q_{CT} and S_{+-} values of these compounds compared to those of the MR-TADF acceptor moiety only. When analyzing the nature of the S_2 state of these compounds, we observed both D_{CT} and q_{CT} increasing with respect to S_1 while S_{+-} decreased. Among the different compounds, ***m*'-AC-DBNA** has a smaller D_{CT} (S_1 1.84 Å, S_2 1.76 Å), but this is readily explained by the symmetry of this compound, which usually biases the D_{CT}. However, based on q_{CT} and S_{+-}, we confirm the long-range CT character of the S_2 state.[63] Each material had a difference density pattern for the S_2 state that is reminiscent of a long-range CT state. **ADBNA-Me-MesNMe2** and **ADBNA-Me-Mes-MesNMe2** have the same electron-accepting MR-TADF moiety. **ADBNA-Me-Mes** has D_{CT} of 1.34 Å, q_{CT} of 0.63 and S_{+-} of 0.94, values all similar to those calculated for other MR-TADF emitters. The S_1 state of **ADBNA-Me-MesNMe2** and **ADBNA-Me-Mes-MesNMe2** are assigned as SRCT, while S_2 has long-range CT character. Finally, **QAO-Dad**, which

contains a **DiKTa** accepting moiety, has D_{CT}, q_{CT} and S_{+-} values all consistent with an S_1 state of SRCT character while S_2 is of long-range CT character.

Another element that could drive the S_1-S_2 state inversion is the potential difference in geometry relaxation energy in the excited state that could exist between SRCT and long-range CT states and which is neglected in vertical excitation calculations. Thus, in polar media, a broad CT emission could be observed, whereas the gas phase calculations predict a S_1 state with a SRCT. (Figure **S73**). Owing to their large S_1-S_2 energy gap (0.52 eV) both **ADBNA-Me-MesNMe$_2$** and **ADBNA-Me-Mes-MesNMe$_2$**, display experimentally two clear, distinct bands in the solvatochromic screen[26] as exemplified by the emission spectrum of **ADBNA-Me-Mes-MesNMe$_2$** in CH_2Cl_2 where dual emission is observed. We assign the high energy band to emission from the SRCT state as it is of similar energy to other structurally similar MR-TADF emitters in the study, and the second low energy band to the CT emission. This example illustrates the importance of modelling both the S_1 and S_2 states of this class of compound.

Table **4**. Calculated excited state S_1 and S_2 energies and their associated CT descriptors for D-A emitters incorporating a MR-TADF core as an acceptor as well the MR-TADF core alone.

	S_1					S_2				
Compound	**Energy / eV**	**D_{CT} / Å**	**q_{CT}**	**S_{+-}**	**Excited state**	**Energy / eV**	**D_{CT} / Å**	**q_{CT}**	**S_{+-}**	**Excited state**
DOBNA	3.68	1.57	0.58	0.92	SRCT	N/A	N/A	N/A	N/A	N/A
ADBNA-Me-Mes	3.04	1.34	0.63	0.94	SRCT	N/A	N/A	N/A	N/A	N/A
DiKTa	3.45	1.45	0.59	0.91	SRCT	N/A	N/A	N/A	N/A	N/A
m'-AC-DBNA	3.56	1.84	0.61	0.89	SRCT	3.69	1.76	0.95	0.62	CT
QAO-DAd	3.37	1.17	0.59	0.93	SRCT	3.45	5.12	0.91	0.33	CT
TBNA-Ac	3.57	1.14	0.59	0.95	SRCT	3.61	5.28	0.95	0.24	CT
TBNA-Di	3.56	1.45	0.59	0.93	SRCT	3.69	5.12	0.62	0.62	CT
ADBNA-Me-MesNMe2 (6b)	3.05	1.29	0.63	0.94	SRCT	3.57	1.73	0.91	0.67	CT
ADBNA-Me-Mes-MesNMe2 (6a)	3.04	1.31	0.63	0.94	SRCT	3.56	4.97	0.92	0.37	CT
TMCz-BO	3.65	1.37	0.58	0.95	SRCT	3.81	5.51	0.95	0.34	CT
TMCz-3P	3.58	1.42	0.59	0.94	SRCT	3.74	5.8	0.93	0.24	CT
M3CzB	3.61	1.01	0.58	0.97	SRCT	3.78	5.70	0.74	0.47	CT

Conclusions

Using TD(A)-DFT and SCS-CC2 calculations we have investigated MR-TADF emitters and materials bearing a MR-TADF core as acceptors in an effort to establish an accurate methodology to predict both ΔE_{ST} and the nature of the low-lying excited states of these compounds. Reaffirming our previous work, we demonstrate the robustness of the ΔE_{ST} prediction when applying the SCS-CC2 method in comparison to TD(A)-DFT, as evidenced by the extremely small MAD value of 0.04 eV reported across 35 MR-TADF emitters. The overestimation observed at the TD(A)-DFT level is consistent for the set of functionals investigated and we assigned it to the poorly predicted S_1 energy due to the absence of

double excitation in TD(A)-DFT impeding an accurate account of Coulomb electron correlation. We would encourage the community with an interest in the design of MR-TADF materials to ensure they employ a computational methodology that includes (at least partially) double excitation to both improve excited state energy prediction as well as the description of the assigned excited state nature. With SCS-CC2, our method of choice, we observe a decrease in ΔE_{ST} when electron delocalisation is increased, and when boron is used in place of ketone. We also characterized the higher-lying S_2 and T_2 excited states, which appear to be in most cases much higher in energy compared to the lower-lying singlet and triplet excited states. Unlike conventional D-A TADF materials, there are only a small fraction of MR-TADF materials that display energetically closely-lying triplet states, whose involvement are believed to facilitate RISC. The slow k_{RISC} measured experimentally for most of the compounds are supported by the very large T_1-T_2, S_1-T_2 and S_1-S_2 energy gaps, suggesting that a spin-vibronic mechanism as observed in D-A TADF is inefficient in MR-TADF compounds. This potentially supports alternative routes for MR-TADF triplet harvesting which have recently been proposed *via* host-guest exciplex state. Owing to the computational cost of wavefunction-based approaches, we anticipate that the community might be reluctant to adopt such an approach, often preferring TD(A)-DFT. TD(A)-DFT not only fails in predicting the excited states energies but it also fails in disclosing the nature of S_1 for most of the functionals with the exception of CAM-B3LYP. In compounds containing a MR-TADF core that acts as an acceptor in D-A TADF emitters, we demonstrated that gas-phase SCS-CC2 calculations predicts S_1 and S_2 to be always of SRCT and long-range CT character, respectively. Because of the high dependence of the emission properties as a function of the polarity of the solvent in these compounds, it is possible that there is a switch from the narrow SRCT-like to a broad CT-like emission. We therefore conclude that a proper account of solvent effects as implemented recently in antiadiabatic approaches that go beyond commonly used (adiabatic) continuum models,[64] and excited states geometry relaxation are required in order to account for the potential S_1-S_2 state inversion between the SCRT and the long-range CT excited states in this class of compounds.

Supporting Information

Photophysical and device data of studied emitters and supplementary computational data of all studied emitters along with coordinates.

Acknowledgments

The St Andrews team would like to thank the Leverhulme Trust (RPG-2016-047) for financial support. E. Z.-C. is a Royal Society Leverhulme Trust Senior Research fellow (SRF\R1\201089). Computational resources have been provided by the Consortium des Équipements de Calcul Intensif (CÉCI), funded by the Fonds de la Recherche Scientifiques de Belgique (F.R.S.-FNRS) under Grant No. 2.5020.11, as well as the Tier-1 supercomputer of the Fédération Wallonie-Bruxelles, infrastructure funded by the Walloon Region under the grant agreement n1117545. Y.O. acknowledges funding by the Fonds de la Recherche Scientifique-FNRS under Grant n° F.4534.21 (MIS-IMAGINE). D.B. is a FNRS Research Director.

References

1. M. Y. Wong and E. Zysman-Colman, *Adv. Mater.,* 2017, **29**, 1605444.
2. Y. Liu, C. Li, Z. Ren, S. Yan and M. R. Bryce, *Nat. Rev. Mater.,* 2018, **3**, 18020.
3. Z. Yang, Z. Mao, Z. Xie, Y. Zhang, S. Liu, J. Zhao, J. Xu, Z. Chi and M. P. Aldred, *Chem. Soc. Rev.,* 2017, **46**, 915.
4. H. Uoyama, K. Goushi, K. Shizu, H. Nomura and C. Adachi, *Nature,* 2012, **492**, 234.
5. Y. Tao, K. Yuan, T. Chen, P. Xu, H. Li, R. Chen, C. Zheng, L. Zhang and W. Huang, *Adv. Mater.,* 2014, **26**, 7931.
6. G. Hong, X. Gan, C. Leonhardt, Z. Zhang, J. Seibert, J. M. Busch and S. Brase, *Adv. Mater.,* 2021, **33**, e2005630.
7. M. K. Etherington, J. Gibson, H. F. Higginbotham, T. J. Penfold and A. P. Monkman, *Nat. Commun.,* 2016, **7**, 13680.
8. M. Moral, L. Muccioli, W. J. Son, Y. Olivier and J. C. Sancho-García, *J. Chem. Theory Comput.,* 2015, **11**, 168.
9. S. Huang, Q. Zhang, Y. Shiota, T. Nakagawa, K. Kuwabara, K. Yoshizawa and C. Adachi, *J. Chem. Theory Comput.,* 2013, **9**, 3872.
10. D. Jacquemin, A. Planchat, C. Adamo and B. Mennucci, *J. Chem. Theory Comput.,* 2012, **8**, 2359.
11. H. Sun, C. Zhong and J.-L. Brédas, *J. Chem. Theory Comput.,* 2015, **11**, 3851.
12. A. D. Becke, *J. Chem. Phys.,* 1993, **98**, 1372.
13. C. Adamo and V. Barone, *J. Chem. Phys.,* 1999, **110**, 6158.
14. T. Cardeynaels, S. Paredis, J. Deckers, S. Brebels, D. Vanderzande, W. Maes and B. Champagne, *Phys. Chem. Chem. Phys.,* 2020, **22**, 16387.
15. Y. Zhao and D. G. Truhlar, *Theor. Chem. Acc.,* 2008, **120**, 215.

16. T. Hatakeyama, K. Shiren, K. Nakajima, S. Nomura, S. Nakatsuka, K. Kinoshita, J. Ni, Y. Ono and T. Ikuta, *Adv. Mater.,* 2016, **28**, 2777.
17. S. Madayanad Suresh, D. Hall, D. Beljonne, Y. Olivier and E. Zysman-Colman, *Adv. Funct. Mater.,* 2020, **30**, 1908677.
18. D. Hall, S. M. Suresh, P. L. dos Santos, E. Duda, S. Bagnich, A. Pershin, P. Rajamalli, D. B. Cordes, A. M. Z. Slawin, D. Beljonne, A. Köhler, I. D. W. Samuel, Y. Olivier and E. Zysman-Colman, *Adv. Opt. Mater.,* 2020, **8**, 1901627.
19. G. Ricci, E. San-Fabian, Y. Olivier and J. C. Sancho-Garcia, *ChemPhysChem,* 2021, **22**, 553.
20. J. Sanz-Rodrigo, G. Ricci, Y. Olivier and J. C. Sancho-Garcia, *J. Phys. Chem. A.,* 2021, **125**, 513.
21. J. Sanz-Rodrigo, Y. Olivier and J. C. Sancho-Garcia, *Molecules,* 2020, **25**.
22. A. Pershin, D. Hall, V. Lemaur, J. C. Sancho-Garcia, L. Muccioli, E. Zysman-Colman, D. Beljonne and Y. Olivier, *Nat. Commun.,* 2019, **10**, 597.
23. A. Hellweg, S. A. Grun and C. Hattig, *Phys. Chem. Chem. Phys.,* 2008, **10**, 4119.
24. A. Tajti, B. Kozma and P. G. Szalay, *J. Chem. Theory Comput.,* 2021, **17**, 439.
25. O. Christiansen, H. Koch and P. J¢rgensen, *Chem. Phys. Lett.,* 1995, **243**, 409
26. J. A. Knoller, G. Meng, X. Wang, D. Hall, A. Pershin, D. Beljonne, Y. Olivier, S. Laschat, E. Zysman-Colman and S. Wang, *Angew. Chem. Int. Ed.,* 2020, **59**, 3156.
27. S. M. Suresh, E. Duda, D. Hall, Z. Yao, S. Bagnich, A. M. Z. Slawin, H. Bassler, D. Beljonne, M. Buck, Y. Olivier, A. Kohler and E. Zysman-Colman, *J. Am. Chem. Soc.,* 2020, **142**, 6588.
28. D. Sun, S. M. Suresh, D. Hall, M. Zhang, C. Si, D. B. Cordes, A. M. Z. Slawin, Y. Olivier, X. Zhang and E. Zysman-Colman, *Mater. Chem. Front.,* 2020, **4**, 2018.
29. N. O. C. Winter and C. Hättig, *J. Chem. Phys.,* 2011, **134**, 184101.
30. H. Tanaka, S. Oda, G. Ricci, H. Gotoh, K. Tabata, R. Kawasumi, D. Beljonne, Y. Olivier and T. Hatakeyama, *Angew. Chem. Int. Ed.,* 2021.
31. I. Kim, K. H. Cho, S. O. Jeon, W.-J. Son, D. Kim, Y. M. Rhee, I. Jang, H. Choi and D. S. Kim, *JACS Au,* 2021, **1**, 987.
32. X. Wu, B.-K. Su, D.-G. Chen, D. Liu, C.-C. Wu, Z.-X. Huang, T.-C. Lin, C.-H. Wu, M. Zhu, E. Y. Li, W.-Y. Hung, W. Zhu and P.-T. Chou, *Nat. Photonics,* 2021, **15**, 780.
33. T. Yanai, D. P. Tew and N. C. Handy, *Chem. Phys. Lett.,* 2004, **393**, 51.
34. O. A. Vydrov and G. E. Scuseria, *J. Chem. Phys.,* 2006, **125**, 234109.
35. O. A. Vydrov and G. E. Scuseria, *J. Chem. Phys.,* 2006, **125**, 234109.
36. Y. Shu and B. G. Levine, *J. Chem. Phys.,* 2015, **142**, 104104.
37. T. J. Penfold, *J. Phys. Chem. C,* 2015, **119**, 13535.
38. M. J. Frisch, G. W. Trucks, H. B. Schlegel, G. E. Scuseria, M. A. Robb, J. R. Cheeseman, G. Scalmani, V. Barone, G. A. Petersson, H. Nakatsuji, X. Li, M. Caricato, A. V. Marenich, J. Bloino, B. G. Janesko, R. Gomperts, B. Mennucci, H. P. Hratchian, J. V. Ortiz, A. F. Izmaylov, J. L. Sonnenberg, Williams, F. Ding, F. Lipparini, F. Egidi, J. Goings, B. Peng, A. Petrone, T. Henderson, D. Ranasinghe, V. G. Zakrzewski, J. Gao, N. Rega, G. Zheng, W. Liang, M. Hada, M. Ehara, K. Toyota, R. Fukuda, J. Hasegawa, M. Ishida, T. Nakajima, Y. Honda, O. Kitao, H. Nakai, T. Vreven, K. Throssell, J. A. Montgomery Jr., J. E. Peralta, F. Ogliaro, M. J. Bearpark, J. J. Heyd, E. N. Brothers, K. N. Kudin, V. N. Staroverov, T. A. Keith, R. Kobayashi, J. Normand, K. Raghavachari, A. P. Rendell, J. C. Burant, S. S. Iyengar, J. Tomasi, M. Cossi, J. M. Millam, M. Klene, C. Adamo, R. Cammi, J. W. Ochterski, R. L. Martin, K. Morokuma, O. Farkas, J. B. Foresman and D. J. Fox *Gaussian 16 Rev. A.01*, Wallingford, CT, 2016.
39. *TURBOMOLE V7.4*, TURBOMOLE GmbH, since 2007; avaliable from http://www.turbomole.com: a development of University of Karlsruhe and Forschungszentrum Karlsruhe GmbH, 2017.
40. T. Etienne, X. Assfeld and A. Monari, *J. Chem. Theory Comput.,* 2014, **10**, 3896.
41. T. Etienne, X. Assfeld and A. Monari, *J. Chem. Theory Comput.,* 2014, **10**, 3906.
42. A. Dreuw and M. Head-Gordon, *Chem. Rev.,* 2005, **105**, 4009.
43. M. Yang, I. S. Park and T. Yasuda, *J. Am. Chem. Soc.,* 2020, **142**, 19468.

44. Y. Qi, W. Ning, Y. Zou, X. Cao, S. Gong and C. Yang, *Adv. Funct. Mater.,* 2021.
45. Y. Liu, X. Xiao, Y. Ran, Z. Bin and J. You, *Chem. Sci.,* 2021, **12**, 9408.
46. X. Cai, Y. Xu, Q. Wang, C. Li and Y. Wang, *ChemRxiv. Preprint,* 2021, 10.26434/chemrxiv.14371073.v1.
47. Y. Olivier, J. C. Sancho-Garcia, L. Muccioli, G. D'Avino and D. Beljonne, *J. Phys. Chem. Lett.,* 2018, **9**, 6149.
48. M. Savarese, C. A. Guido, E. Brémond, I. Ciofini and C. Adamo, *The Journal of Physical Chemistry A,* 2017, **121**, 7543.
49. K. Stavrou, A. Danos, T. Hama, T. Hatakeyama and A. Monkman, *ACS Appl. Mater. Interfaces,* 2021, **13**, 8643.
50. L.-S. Cui, A. J. Gillett, S.-F. Zhang, H. Ye, Y. Liu, X.-K. Chen, Z.-S. Lin, E. W. Evans, W. K. Myers, T. K. Ronson, H. Nakanotani, S. Reineke, J.-L. Bredas, C. Adachi and R. H. Friend, *Nat. Photonics,* 2020, **14**, 636.
51. E. Zysman-Colman, *Nat. Photonics,* 2020, **14**, 593.
52. H. Noda, X.-K. Chen, H. Nakanotani, T. Hosokai, M. Miyajima, N. Notsuka, Y. Kashima, J.-L. Brédas and C. Adachi, *Nat. Mater.,* 2019, **18**, 1084.
53. H. Min, I. S. Park and T. Yasuda, *Angew. Chem. Int. Ed.,* 2021, **60**, 7643.
54. T. Northey and T. J. Penfold, *Org. Electron.,* 2018, **59**, 45.
55. H. J. Kim, M. Godumala, S. K. Kim, J. Yoon, C. Y. Kim, H. Park, J. H. Kwon, M. J. Cho and D. H. Choi, *Adv. Opt. Mater.,* 2020, **8**, 1902175.
56. G. Meng, X. Chen, X. Wang, N. Wang, T. Peng and S. Wang, *Adv. Opt. Mater.,* 2019, **7**, 1900130.
57. Y. Yuan, X. Tang, X. Y. Du, Y. Hu, Y. J. Yu, Z. Q. Jiang, L. S. Liao and S. T. Lee, *Adv. Opt. Mater.,* 2019, **7**, 1801536.
58. H. Hirai, K. Nakajima, S. Nakatsuka, K. Shiren, J. Ni, S. Nomura, T. Ikuta and T. Hatakeyama, *Angew. Chem. Int. Ed.,* 2015, **54**, 13581.
59. D. Karthik, D. H. Ahn, J. H. Ryu, H. Lee, J. H. Maeng, J. Y. Lee and J. H. Kwon, *J. Mater. Chem. C.,* 2020, **8**, 2272.
60. D. Song, Y. Yu, L. Yue, D. Zhong, Y. Zhang, X. Yang, Y. Sun, G. Zhou and Z. Wu, *J. Mater. Chem. C.,* 2019, **7**, 11953.
61. J. U. Kim, I. S. Park, C. Y. Chan, M. Tanaka, Y. Tsuchiya, H. Nakanotani and C. Adachi, *Nat. Commun.,* 2020, **11**, 1765.
62. D. H. Ahn, S. W. Kim, H. Lee, I. J. Ko, D. Karthik, J. Y. Lee and J. H. Kwon, *Nat. Photonics,* 2019, **13**, 540.
63. Y. Olivier, B. Yurash, L. Muccioli, G. D'Avino, O. Mikhnenko, J. C. Sancho-García, C. Adachi, T. Q. Nguyen and D. Beljonne, *Phys. Rev. Mater.,* 2017, **1**, 075602.
64. D. K. A. Phan Huu, R. Dhali, C. Pieroni, F. Di Maiolo, C. Sissa, F. Terenziani and A. Painelli, *Phys. Rev. Lett.,* 2020, **124**, 107401.

TOC – 35 MR-TADF emitters have been modelled comparing TD(A)-DFT with SCS-CC2. The deviation in terms of ΔE_{ST} values calculated compared to experimental data is very small with SCS-CC2 in strong contrast with TD(A)-DFT.

Multi-resonant TADF emitters, an in-depth computational study